Microsc. Microanal. Microstruct. **3** (1992) 415–431 OCTOBER **1992**, PAGE 415

Classification
Physics Abstracts
61.16D

HREM investigation of $n = 4$ members of the tubular bismuth cuprates $(Bi_{2+x}Sr_{2-x}CuO_6)_n$ $(Sr_8Cu_6O_{16+y})$

Bernadette Domengès([1]), Maria Teresa Caldes([1]), Maryvonne Hervieu([1]), Amparo Fuertes([2]) and Bernard Raveau([1])

([1]) Laboratoire de Cristallographie et Sciences des Matériaux, Bd. du Maréchal Juin, 14050 Caen Cedex, France
([2]) Institut de Ciencias de Materials de Barcelona (C.S.I.C.), Campus UAB-08193-Bellaterra, Barcelona, Spain

(Received June 28, 1992; accepted November 02, 1992)

Abstract. — The HREM study of the fourth members of the tubular bismuth cuprates family, $Bi_4Sr_8Cu_5O_{19}$, $Bi_4Sr_7LaCu_5O_{19.5}$ and $Bi_4Sr_8Cu_3Fe_2O_{20}$ is performed. The microstructure of most crystals is characterized by domains showing a regular atom stacking. A new monoclinic-5 tubular structure is identified twice in large domains.

1. Introduction.

After the observation of superconductivity in the Bi-Sr-Cu-O system [1], the exploration of the latter has shown its extraordinarily rich chemistry. Besides the **2201** modulated oxides, superconducting or not [2-4], a **2201**-monoclinic phase, called collapsed **2201** [5] has also been isolated. The discovery of the orthorhombic oxide $Bi_4Sr_8Cu_5O_{19}$ [6], with a tunnel structure has opened the route to the research of a large series of cuprates. In fact this oxide represents the member $n = 4$ of the large structural family $(Bi_{2+x}Sr_{2-x}CuO_6)_n$ $(Sr_8Cu_6O_{16+y})$, called orthorhombic tubular phases [7], for which numerous domains and boundaries were evidenced by high resolution electron microscopy [8]. Besides these numerous oxides a new form of the seventh member of the above family, but with a monoclinic symmetry was isolated [9]. The X-ray and neutron diffraction powder studies of the $n = 4$ members of the tubular phases, $Bi_4Sr_8Cu_5O_{19+y}$ [6], $Bi_4Sr_{8-x}La_xCu_5O_{19+y}$ [10] and $Bi_4Sr_8Cu_3Fe_2O_{19+y}$ [11] let appear, in spite of their great similarities, some structural differences between each compound. We report here on the high resolution electron microscopy investigation of these $n = 4$ tubular phases.

2. Experimental.

The cuprates with nominal compositions $Bi_4Sr_8Cu_5O_{19}$, $Bi_4Sr_7LaCu_5O_{19.5}$ and $Bi_4Sr_8Cu_3Fe_2O_{20}$ were synthesized according to the procedure previously reported [7, 10, 12].

For electron microscopy study, the samples were softly ground in n-butanol and deposited on a holey carbon coated copper grid. The electron diffraction work was performed on JEM 200CX equipped with a top-entry (± 10°) goniometer and an objective lens of spherical aberration constant $C_s = 0.8$ mm. Image calculations were performed using the multislice method of EMS program [13].

3. Structural recalls.

The structure of the orthorhombic tubular phase, fourth member of the family $(Bi_{2+x}Sr_{2-x}Cu_2O_6)_n$ $(Sr_8Cu_6O_{16+y})$ (Fig. 1a) derives from the **2201**-$Bi_2Sr_2CuO_{6+\delta}$ modulated phase (Fig. 1b) by the intergrowth with $[Sr_8Cu_6O_{16+y}]$ perovskite related slices perpendicularly to the copper layers of the **2201**-type structure. In fact these $Bi_4Sr_8Cu_5O_{19}$ orthorhombic tubular phases consist of **2201**-type slices, which are four CuO_6 octahedron wide along **b**, i.e. involve four $[BiO]_\infty$ double rows running along **a** (Fig. 1a). Such slices can be formulated $[(Bi_2Sr_2CuO_6)_4]_\infty$ in agreement with their similarity with the $Bi_2Sr_2CuO_6$-type structure. The association of these quadruple **2201**-type slices with the $Sr_8Cu_6O_{16}$ slices prevents the modulation of the structure contrary to the $Bi_2Sr_2CuO_6$ structure in which one observes a waving of the $[BiO]_\infty$ layers. In order to make easier the discussion of the relationships and defects between the different phases of the system, we can use a schematic representation of the structure omitting oxygen atoms (Fig. 1c), in which vertical or horizontal bars represent the Sr-Cu-Sr sticks of the CuO_6 octahedra, large dots correspond to Bi of the $[BiO]_\infty$ rows, and squares correspond to the crossing of $[Sr_8Cu_6O_{16+y}]_\infty$ slices with the copper layers, forming the square pillar unit $[Sr\text{-}Cu\text{-}Sr]_4$ where copper may exhibit a five-fold or four-fold coordination; in the case of the modulated **2201** structure, one only observes layers of undulating vertical bars corresponding, to the single octahedral copper layers, alternating with undulating layers of double dots corresponding to the double $[BiO]_\infty$ layers (Fig. 1d). Thus, in this representation, the different n-members of the orthorhombic tubular phases are characterized by the size of Bi block represented by $n \times 2$ large dots or by the number n of vertical bars which are observed between two successive squares.

Besides the orthorhombic tubular phases, there exist monoclinic tubular cuprates which can be deduced from the orthorhombic one by translating a copper layer of about 2.7 Å. This is the case of the $n = 7$ monoclinic member [9] whose structural model (Fig. 2a) differs from the orthorhombic one (Fig. 2b) by the nature of the $[Sr_8Cu_6O_{16-y}]_\infty$ slice which do not involve corner-sharing CuO_6 octahedra but double rows of corner-sharing CuO_5 pyramids (Fig. 2a) or edge-sharing CuO_6 octahedra running along **a**. The schematic representation of such a monoclinic $n = 7$ structure is given in figure 2c.

4. Results and discussion.

The electron diffraction study of La- and Fe- substituted samples agreed with the $n = 4$ tubular phase - i.e. space group Bbab with $a \approx 0.54$ nm, $b \approx 3.4$ nm, $c \approx 2.4$ nm (Fig. 3). No special phenomenon could be related to substitution of La for Sr or Fe for Cu, in agreement with the structure resolution work [6, 10 11]. E.D. pattern with splitted dots forming arcs were often observed and could be related to misoriented domains, the corresponding images showing Moire patterns at the junction and/or superimposition of the domains.

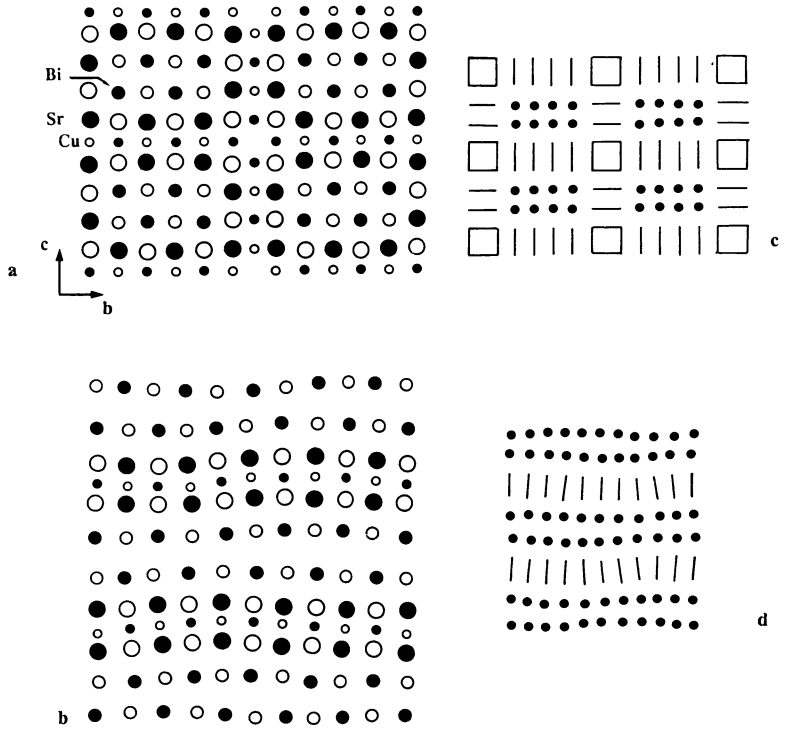

Fig. 1. — (100) projections of a) $Bi_4Sr_8Cu_5O_{19}$ structure and b) modulated $Bi_2Sr_2CuO_6$ structure; oxygen atoms are omitted, as in the following drawings of this paper. Corresponding schematic representation of these structures c) $n = 4$ tubular and d) modulated **2201.**

For the high resolution electron microscopy study about ten crystals of each tubular phases, $Bi_4Sr_8Cu_5O_{19}$, $Bi_4Sr_7LaCu_5O_{19.5}$ and $Bi_4Sr_8Fe_2Cu_3O_{20}$ were investigated. The electron beam was most often parallel to [100] direction, which gives the best description of the structure (Fig. 1). Some observations were also made with the electron beam parallel to [001], which allows to detect stacking fault parallel to the [100] direction.

THE REGULAR STACKING OF THE CATIONS. — Considering (100) images, no significant variation of contrast was observed from $Bi_4Sr_8Cu_5O_{19}$ crystals to La- or Fe- substituted ones. Images calculations were performed based on the neutron diffraction structure resolution data [6, 10, 11]. The comparison of calculated through-focus series for $Bi_{4.2}Sr_{7.8}Cu_5O_{19.5}$, $Bi_4Sr_7LaCu_5O_{20.3}$ and $Bi_4Sr_8Fe_2Cu_3O_{19.3}$ confirmed previous remark. Most of the images of the through-focus series (Fig. 4a) give a "brick-wall" like contrast emphasizing the building principle of the tubular structure. Indeed, to begin with the "joint at each corner of the brick", the pillar unit [Sr-Cu-Sr]$_4$ is most often easily distinguished, either under the form of four dots in square corresponding to Sr atoms (for focus values close to −5 or −65 nm, i.e. high electron density highlighted) or under the form of a bright dot corresponding to the O atom at the center of the pillar (focus close to −35 or −125 nm i.e. low electron density highlighted). The perovskite related slices of the structure which intersect at the pillar unit will then appear as bright dots (for Sr atoms in the first type of images) or grey dots (for O atoms in the second type). Then, the four $[BiO]_\infty$ double rows, forming the brick itself, will appear either as a group of four by two bright dots in the first case

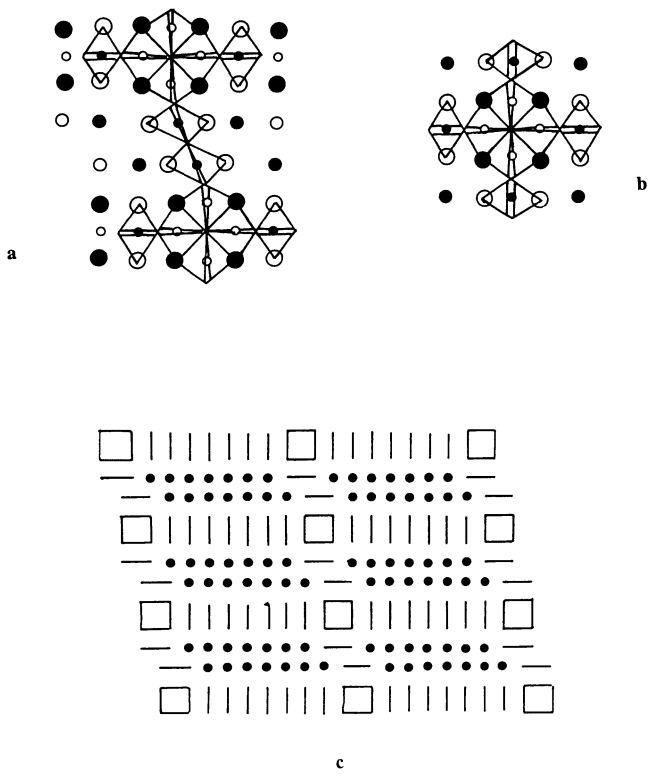

Fig. 2. — (100) projection of perovskite related slice in a) monoclinic $n = 7$ tubular phase and b) orthorhombic tubular phase. c) schematic representation of monoclinic $n = 7$ tubular structure.

or very dark dots in the second one. The calculated series fit well with experimental images. Figure 4b gives some characteristic experimental images of this $n = 4$ member. For -5 nm focus value, the brighter dots correspond to Sr atoms of the perovskite related slices, those of the pillar unit [Sr-Cu-Sr]$_4$ being distinguished; they constitute the "cement" of the brick wall. [BiO]$_\infty$ rows appear as group of four by two slightly greyier dots. For -35 nm focus value, the center of the pillar unit [Sr-Cu-Sr]$_4$ appears as very bright dot, oxygen atoms of the perovskite related slice are slightly less bright and [BiO]$_\infty$ rows are very dark. The image contrast is very sensitive to a slight misorientation of the optical axis of the objective lens which can lead to a dissymmetry of the contrast as observed on given $Bi_4Sr_8Fe_2Cu_3O_{19.3}$ image of figure 4b. Image calculation based on a slightly tilted beam allowed to confirm this fact – calculated images with a beam tilting close to 1 mrad and parallel to **c** are in good agreement with the observed ones.

It is worth pointing out that most of the crystal images show an even contrast, characteristic of the regular stacking of the cations of the $n = 4$ orthorhombic tubular structure, though a monoclinic distortion was observed on HREM images of some crystals (Fig. 4b). This distortion could also be measured on the corresponding E.D. patterns. It appeared to be in the range 0.5° – 1° and could not be related to a main structural change, E.D. dot intensity and image contrast being left characteristic of the $n = 4$ tubular phase. Furthermore, this phenomenon was more often encountered during HREM study in the JEM 200 CX (high voltage : 200 kV) than from E.D. investigation on the JEM 120 CX (high voltage 120 kV) especially $Bi_4Sr_8Cu_5O_{19}$ crystals showed a relative stability under the electron beam. This monoclinic distortion, which origin

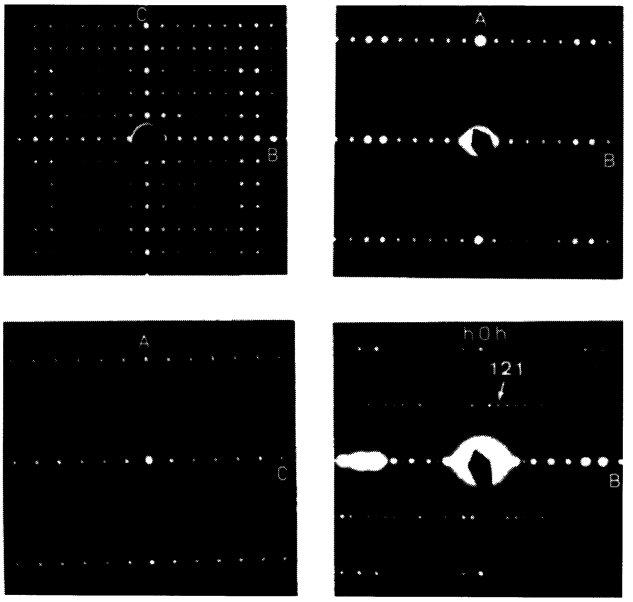

Fig. 3. — Characteristic E.D. patterns of $n = 4$ tubular phase, showing the following existence conditions of Bbab space group : $0kl$, $k = 2n$ ($l = 2n$); $h0l$, $h = 2n$ ($l = 2n$); $hk0$, $k=2n$ ($h = 2n$); hkh, *no condition.*

has no relation with the monoclinic tubular phase structure, may be due to a relaxation of the orthorhombic crystal framework under the electron beam.

5. Extended defects.

In a different way, the relaxation of the framework may lead to a disordering of the cation stacking, which is associated with a disappearance of the square pillar unit [Sr-Cu-Sr]$_4$ as shown from figure 5.

The intergrowth defects are very rare. The only intergrowth defect was observed in a $Bi_4Sr_8Fe_2Cu_3O_{19.3}$crystal as shown from the (001) HREM image (Fig. 6). On regular areas of the crystal, five rows of bright dots alternate with two rows of grey dots. The group of five rows can be assimilated to the low electron density zone – i.e. oxygen atoms of the basal plane of the CuO_6 octahedra of the $(Bi_2Sr_2Cu_6)_4$ units – as observed on similar materials viewed along this direction [14]. The faulty slab is made of seven rows of bright dots. It can thus be interpreted as the (001) projection of a $(Bi_2Sr_2CuO_6)_6$ unit, i.e. one slab of a $n = 6$ member of the orthorhombic tubular phase family. Indeed, the measured width of this slab, close to 2.25 nm corresponds to the $b/2$ parameter of the $n = 6$ member.

Another type of extended defects, deals with the appearance in the $n = 4$ orthorhombic tubular matrix of domains identified as $n = 5$ monoclinic tubular phase. Such domains are shown on the medium magnification images of figure 7 for $Bi_4Sr_8Cu_5O_{19}$ and $Bi_4Sr_7LaCu_5O_{19.5}$ crystals ; the array parameters were measured as 1.92×1.29 nm^2,$\alpha = 100°$, close to the theoretical parameters of the monoclinic $n = 5$ tubular phase ; **b** axes of each domain are almost parallel and **c** axes make an angle of 10°. One recognizes the brick wall-like contrast characteristic of the orthorhombic and monoclinic tubular phases. The enlarged (100) HREM images of $Bi_4Sr_7LaCu_5O_{19.5}$ crys-

$Bi_{4.2}Sr_{7.8}Cu_5O_{19.5}$

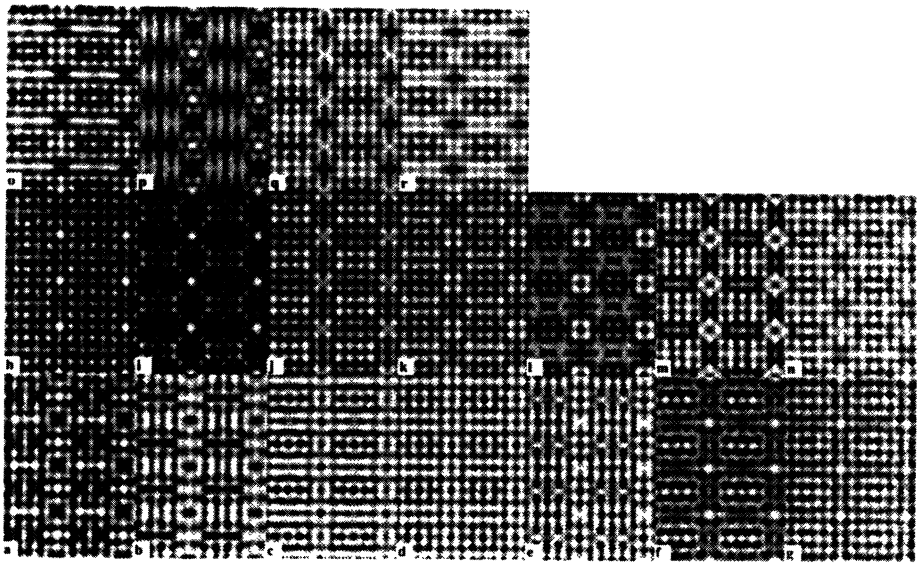

Fig. 4. — a) Calculated through-focus series of $Bi_{4.2}Sr_{7.8}Cu_5O_{19.5}$, $Bi_4Sr_7LaCu_5O_{20.3}$ and $Bi_4Sr_8Fe_2Cu_3O_{19.3}$ structures. Calculation parameters are: high voltage $V = 200$ kV, spherical aberration constant $C_s = 0.8$ mm, focus spread $\Delta = 12$ nm, half convergence angle $\alpha = 0.8$ mrad, objective aperture radius $R = 8\,\text{nm}^{-1}$, thickness $T = 3.2$ nm, focus D_f varies from **a** 25 to **r** −145 nm by 10 nm step. b) Experimental characteristic images; corresponding $Bi_{4.2}Sr_{7.8}Cu_5O_{19.5}$ calculated images, projected potential and schematic reproduction of the structure are joined. Note the monoclinic distortion of experimental images (see text).

tal (Fig. 8) show the easiness of junction between "orthorhombic 4" and "monoclinic 5" tubular phases. The **b** axes of each domain make an angle of 2° which cannot be explained by a small rotation of the monoclinic domain arround the $[01\bar{1}]$ direction, but is probably due to the accomodation of the frameworks, avoiding a too large distortion at the boundary. From this through focus series, one observes that in the monoclinic domain each "brick of the wall" has the same size. As shown from the −35 nm image, where $[BiO]_\infty$ chains parallel to [100] appear as dark dots, each block consists of five double $[BiO]_\infty$ rows; thus the structure of the monoclinic domain could be deduced from that of the orthorhombic $n = 5$ tubular phase (Fig. 9a) by translating each brick of 0.27 nm along **b** (Fig. 9b) so that the mean direction of the perovskite related slices parallel to **c** form an angle close to 100° with **b**. Nevertheless the contrast relative to the copper slices which are parallel to **c** is slightly different in the monoclinic domain from that in the orthorhombic ones, especially at the $[Sr\text{-}Cu\text{-}Sr]_4$ pillar level. For instance, on −5 nm defocus image, a grey contrast is observed in the diagonal of the pillar unit. Several image calculations have shown that this change of contrast cannot be attributed to a misorientation of the crystal and/or thickness effects. Thus, a model based on twice half-pillar unit is proposed for the junction at the crossing of the perovskite related slices, leading to the formation of two facing units made of two trigonal CuO_5 bipyramids sharing an edge (Fig. 9c). As a reference, the variety of geometry of CuO_5 polyhedron has been overviewed by Effenberger [15]. This unit is to be compared to the pillar unit built up from four

$Bi_4Sr_7LaCu_5O_{20.3}$

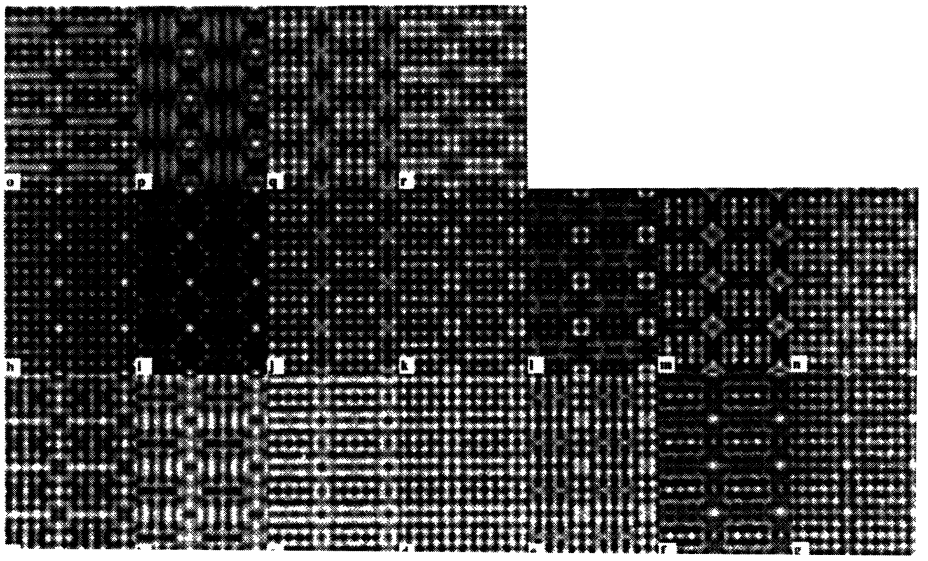

$Bi_4Sr_8Fe_2Cu_3O_{19.3}$

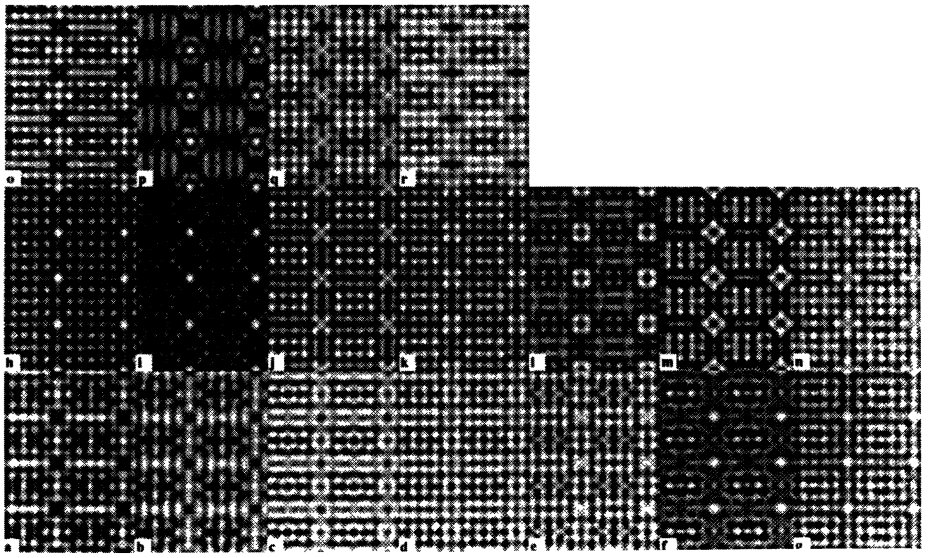

Fig. 4. — a) suite

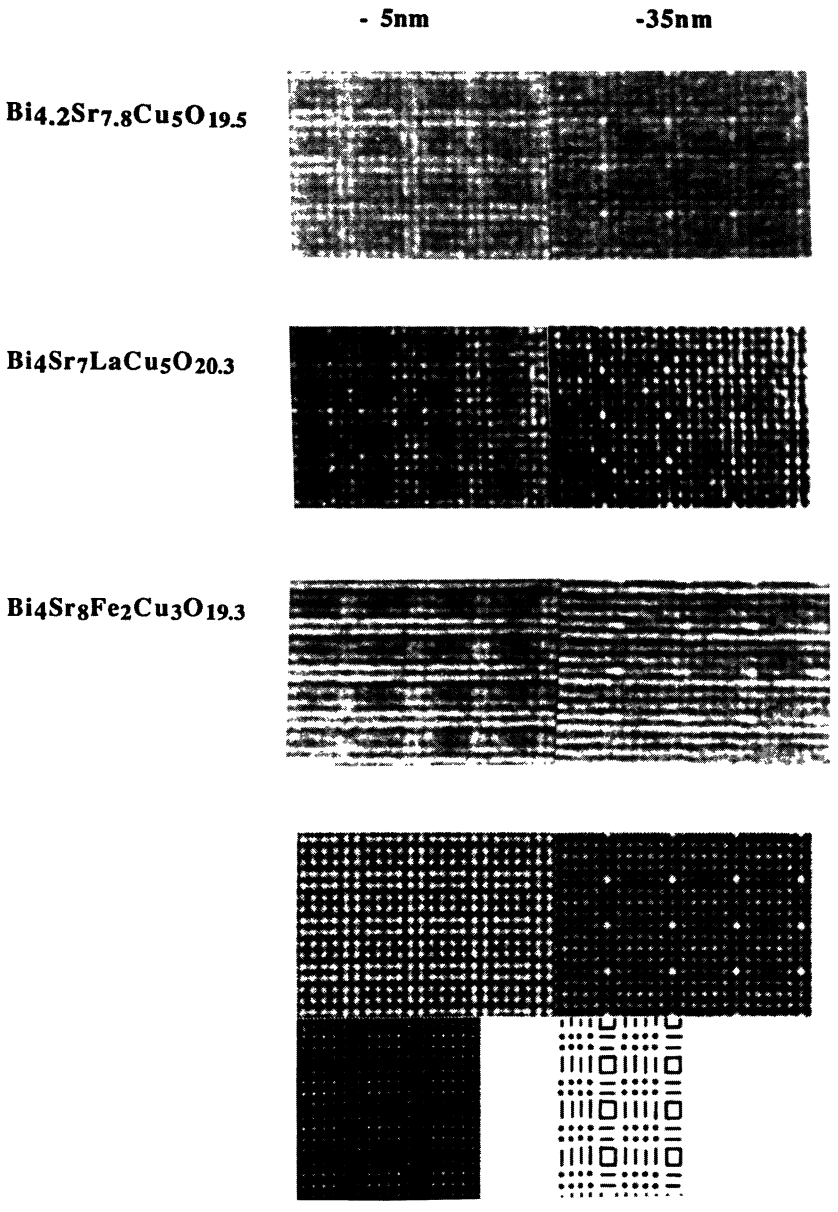

Fig. 4. — b) suite

trigonal CuO_5 bipyramids sharing an edge in the orthorhombic tubular phase (Fig. 2b) or to that in the $n = 7$ monoclinic tubular phase [9] and in the defect proposed by Matsui *et al.* [16] where the pillar unit remains unchanged and two trigonal CuO_5 corner-sharing bipyramids or two edge-sharing CuO_6 octahedra, depending on oxygen content, are formed at the $[Sr\text{-}Cu\text{-}Sr]_2$ unit level (Fig. 2a). Thus, a boundary parallel to (011) plane of orthorhombic tubular 4 structure between an orthorhombic-4 and a monoclinic-5 domains can be proposed (Fig. 10a). Considering this

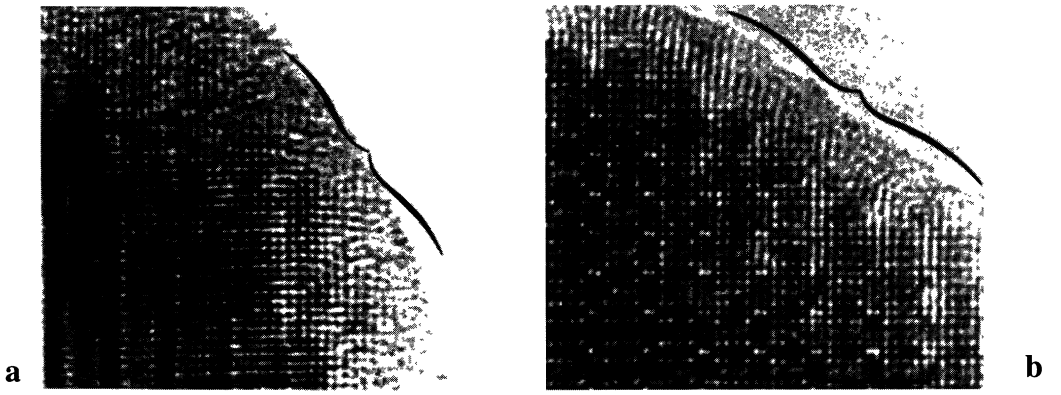

Fig. 5. — HREM images showing disorganization of tubular 4 framework on the thin edge of the crystal: a) La-substituted crystal, (001) projection; b) Fe-substituted crystal, (100) projection.

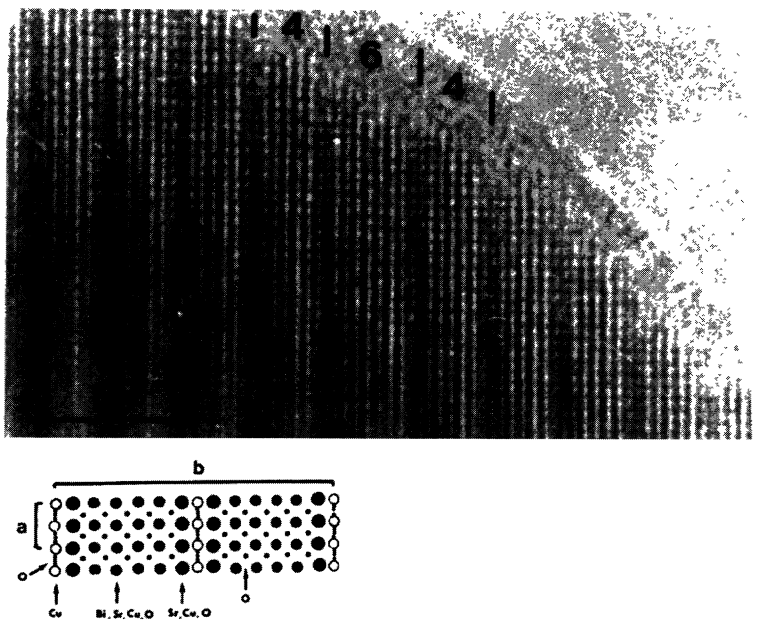

Fig. 6. — (001) HREM image of a Fe-substituted crystal showing a faulty slab corresponding to an $n = 6$ number of the tubular family, (001) projection of the structure is given and the nature of each atom rows parallel to c is precised.

schematic representation, it clearly appears that the (011) plane corresponds to the plane of lowest energy. Indeed, a boundary between a member n_o of the orthorhombic tubular family and a member n_m of the monoclinic tubular family will be planar and parallel to the plane $(01\ l_o)_{n_o\text{-ortho}}$ if the following equation is verified.

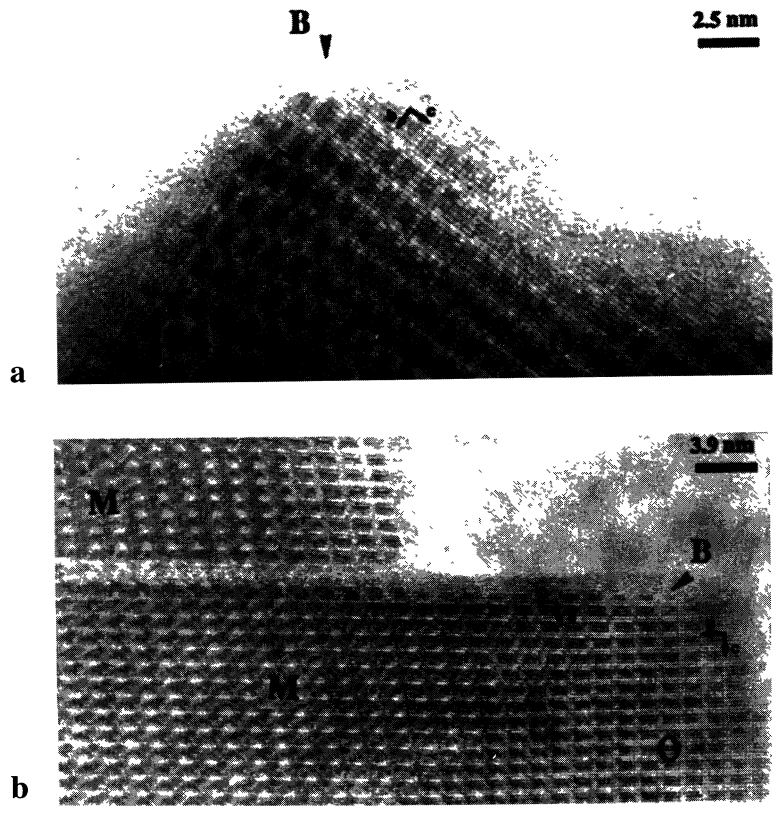

Fig. 7. — Medium magnification (100) HREM images showing monoclinic domains, a) $Bi_4Sr_8Cu_5O_{19}$ and b) La-substituted crystals. A planar boundary (B) is observed between monoclinic (M) and orthorhombic (O) domains.

$$l_o\, L_o = l_m\, L_m - s\, a_p \frac{\sqrt{2}}{2} \qquad l_o, l_m \text{ and } s \text{ integers} \tag{i}$$

L_o and L_m are the length of a "brick" of each domain i.e.

$$L_o = n_o\, a_p \frac{\sqrt{2}}{2} + P \quad \text{and} \quad L_m = n_m\, a_p \frac{\sqrt{2}}{2} + P, \qquad P \approx a_p$$

The term $s\, a_p \frac{\sqrt{2}}{2}$ measures the shifting parallel to $\mathbf{b}_m$ from one "brick" row to the other in the monoclinic domain. Most often $s = \pm 1$ but some examples of higher shifting were observed as defects (7). Equations (i) becomes:

$$l_o\, n_o = l_m\, n_m - s + (l_m - l_o)\sqrt{2} \qquad l_o, l_m, n_o, n_m, s \text{ integers} \tag{ii}$$

This means that $(l_m - l_o)\sqrt{2}$ must be zero, thus $l_m = l_o = l$. Then,

$$n_o = n_m - \frac{s}{l} \tag{iii}$$

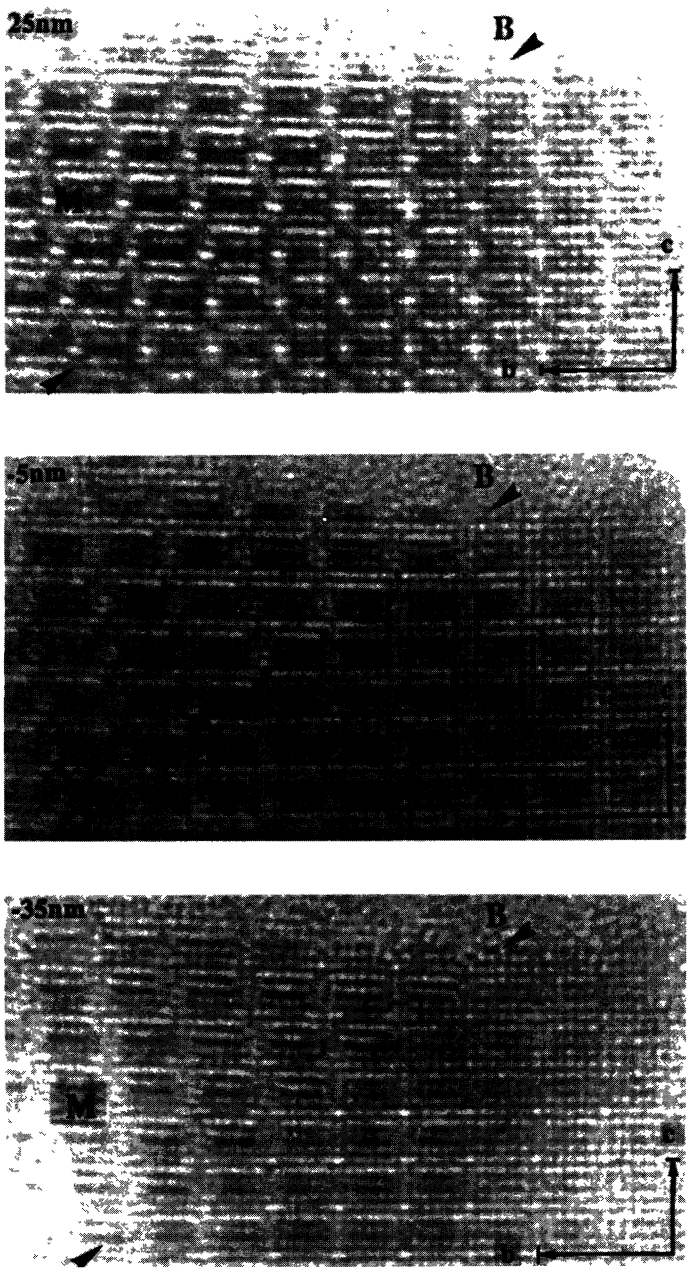

Fig. 8. — Enlarged HREM images of the experimental through-focus series of the edge of previous La-substituted crystal showing the planar boundary (B) between monoclinic (M) and orthorhombic tubular 4 (O) domains; **b** and **c** axes of orthorhombic tubular 4 structure are drawn.

With $s = \pm 1$, l must be equal to 1, thus (iii) becomes : $n_o = n_m \pm 1$.

Consequently a planar boundary can only be obtained between one orthorhombic and one monoclinic domains of two adjacent members e.g. 4-5 and the boundary plane will be $(011)_{ortho}$.

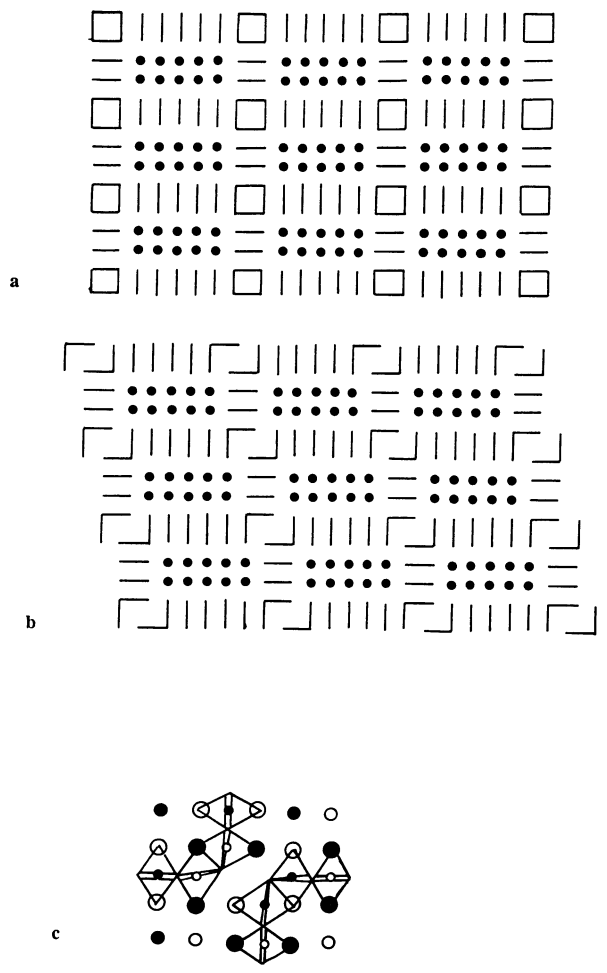

Fig. 9. — a) Schematic representation of orthorhombic tubular 5 structure. b) Schematic representation of the proposed model for monoclinic tubular 5 structure. c) Detailed drawing showing the polyhedra involved at the crossing of perovskite related slices in previous model.

Figure 10b gives an example of planar boundary between an $n_o = 6$ orthorhombic domain and $n_m = 5$ monoclinic one, with $s = -1$.

Another interesting type of defect deals with the intergrowth between tubular phases and modulated **2201.** It was observed in Fe-substituted samples. The first example is given in figure 11. The medium resolution image shows two domains : the first one exhibits the usual "brick wall" contrast of the $n = 4$ tubular phase, the second one exhibits a modulated contrast typical of the **2201** modulated phase, the contrast symmetry being orthorhombic body centered, which indicates a q value close to 4, in agreement with previous studies of the Fe-substituted $Bi_2Sr_2Cu_{1-x}Fe_xO_y$ phase. The SAED pattern of both domains allowed the q_b vector of modulated area to be measured : $q_b \approx 3.9$. This value is slightly smaller than that observed in $Bi_2Sr_2Cu_{0.5}Fe_{0.5}O_y$ [17]. It may thus mean that this modulated domain is Fe-richer, since the limit of the solid solution formation was determined as $x = 0.6 \pm 0.1$ for $Bi_2Sr_2Cu_{1-x}Fe_xO_y$ prepared in air [18]. The domain boundary is parallel to (001) and appears located at the perovskite related slice level. Indeed, the

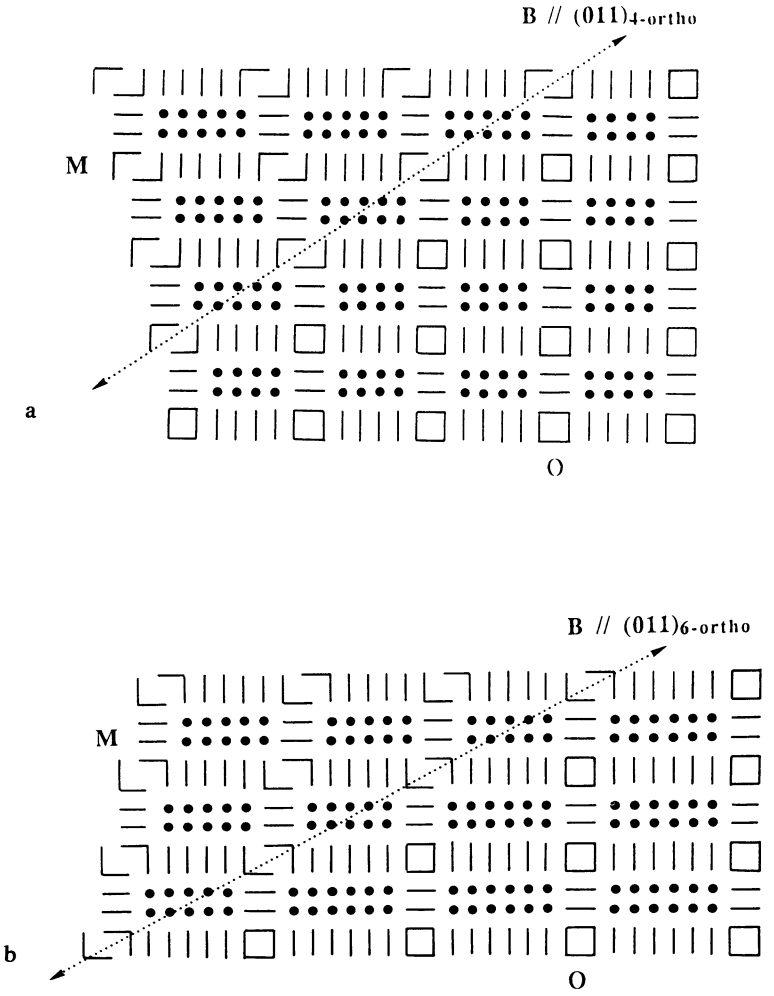

Fig. 10. — Schematic representation of neighboring orthorhombic and monoclinic domains: a) orthorhombic tubular 4 and monoclinic tubular 5, $n_o = 4$, $n_m = 5$, $s = 1$; b) orthorhombic tubular 6 and monoclinic tubular 5, $n_o = 6$, $n_m = 5$, $s = -1$.

model of figure 12 shows the easiness of junction between both frameworks.

The second example shows an $n = 4$ Fe-substituted crystal which exhibits many small domains, slightly misoriented, leading to strong variation of the contrast from one to the other (Fig. 13). This low magnification image shows that the crystal is built up of two main domains translated parallely to **b**, i.e. with a domain boundary parallel to **b**. Enlargement of high resolution images of the boundary (Fig. 14) on a thin edge of the crystal allows its structure to be analysed : the boundary width – measured pillar to pillar (Fig. 14) is around 1.42 ± 0.06 nm, the translation vector of one domain to the other being 1/5 (b_{tub4}) . The analysis of contrast of the through focus series and geometrical considerations suggest that this boundary is made of two rock-salt layers, i.e. three $[(Bi, Sr)O]_\infty$ rows (Fig. 15) which are probably waving in a similar way to those observed in the **2201** modulated structure.

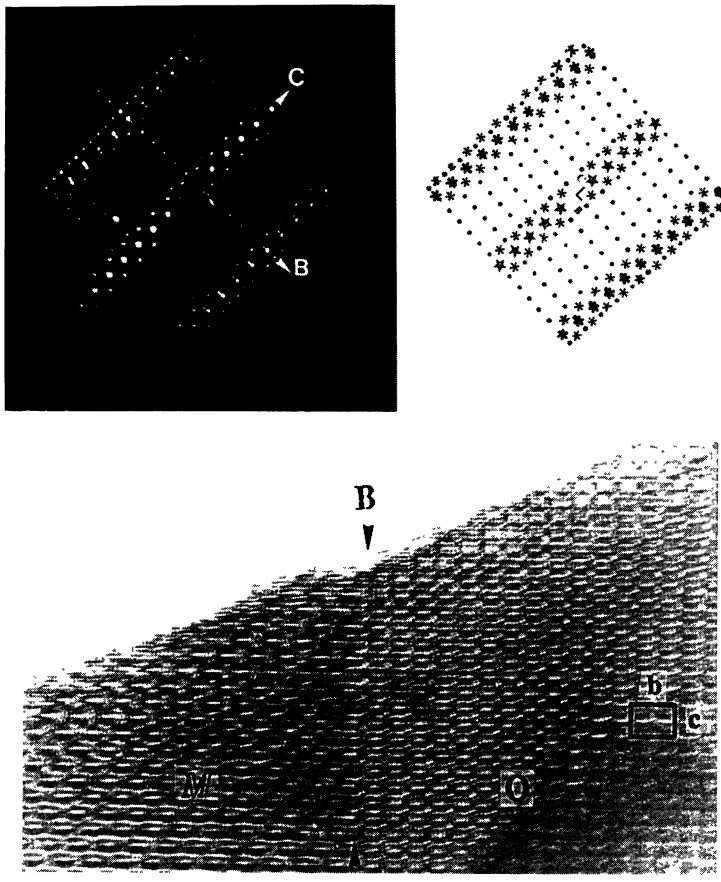

Fig. 11. — (100) medium resolution image and corresponding SAED pattern of a Fe-substituted crystal showing one orthorhombic tubular 4 domain (O) and one modulated **2201** domain (*M*) sharing a planar boundary parallel to (001). On E.D. drawing, dots correspond to (100) tubular pattern and stars to modulated **2201** one.

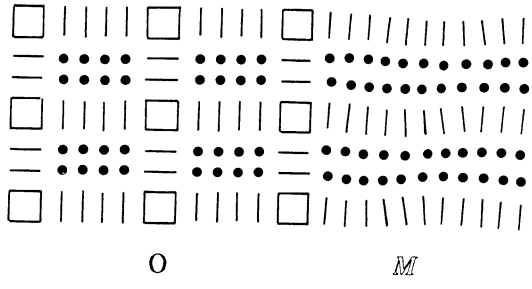

Fig. 12. — Schematic representation showing the easiness of junction between an orthorhombic tubular domain (O) and a modulated **2201** one (*M*) with a (001) planar boundary.

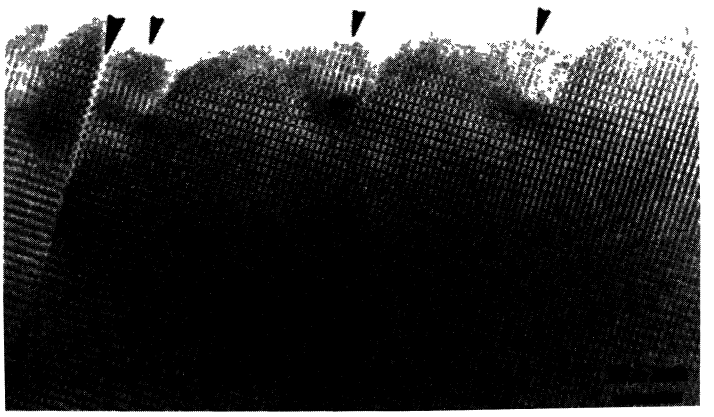

Fig. 13. — (100) medium magnification HREM image of a Fe-substituted crystal showing small domains (small arrows) slightly misoriented and of different thickness. A boundary (big arrow) between two wide domains is also observed.

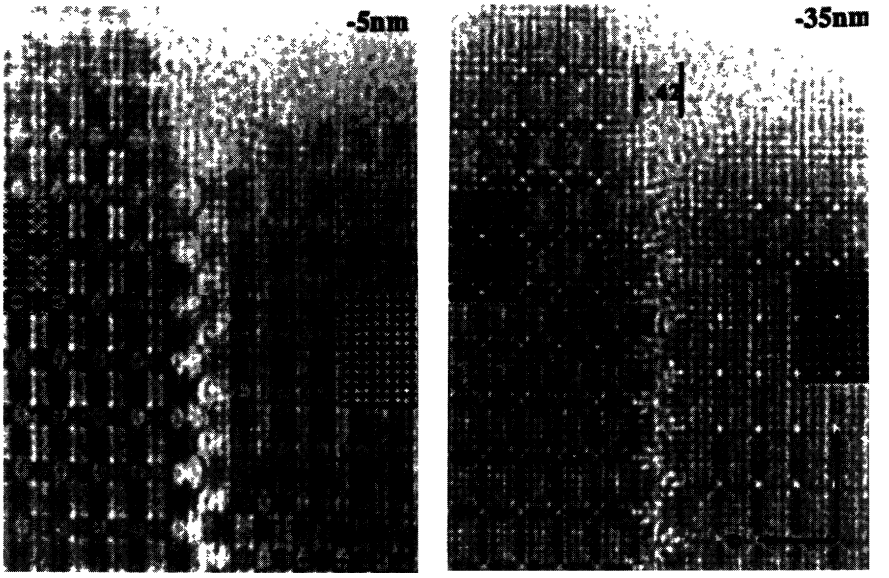

Fig. 14. — Enlargements of HREM images of previous crystal showing detail of the boundary. Calculated images (V, C_s, Δ, α and R parameters are those of Fig. 4a) are inset on each domain ; focus value is close to a) −5 nm and b) −35 nm and thickness close to 7.5 nm for left side domain and 4.3 nm for right side domain. The 1.42 nm-wide boundary shows a modulated contrast.

6. Conclusion.

This HREM study of orthorhombic tubular 4 phases, La and Fe substituted included, did not let

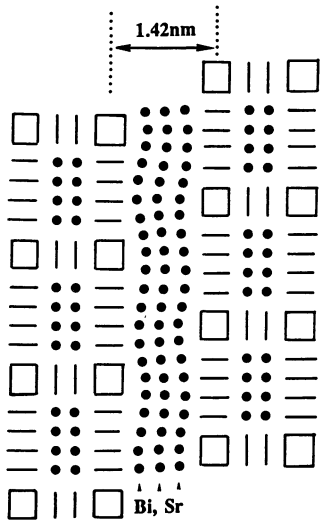

Fig. 15. — Schematic representation of model for previous boundary based on three waving $[(Bi, Sr)O]_\infty$ rows.

appear any peculiar behavior related to the La or Fe substitution. Under a structural point of view, two main defects were observed. A new monoclinic form of tubular structure was observed twice on large domains. It was identified as the monoclinic $n = 5$ member of the tubular family. The close structural relationships between the tubular framework and the **2201** modulated one was emphasized by an observed defect on Fe-substituted crystals. It corresponds to an orthorhombic tubular domain sharing with a **2201** modulated one a planar boundary parallel to (010). Besides these defects, most crystals show domains with an even contrast, characteristic of a regular cation stacking with almost no intergrowth defect with other member of the family. This result do agree with the classical behavior of structures based on the intergrowth of two structural units, one unit being characterized by a variable width : small members usually appear very regular to be opposed to high members which show many intergrowth defects [8].

References

[1] MICHEL C., HERVIEU M., BOREL M.M., GRANDIN A., DESLANDES F., PROVOST J. and RAVEAU B., *Z. Phys. B* **68** (1987) 421.

[2] ROTH R.S., RAWN C.J. and BENDERSKY I.A., *J. Mater. Res.* **5** (1990) 46.

[3] IKEDA Y., ITO H., SHIMOMURA S., OUE Y., INABA K., IROI Z. and TAKANO M., *Physica C* **159** (1989) 93.

[4] CHAKOUMAKOS B.C., EBEY P.S., SALES B.C. and SONDUS E., *J. Mater. Res.* **4** (1991) 767.

[5] HIROI Z., IKEDA Y., TAKANO M. and BANDO Y., *J. Mater. Res.* **6** (1991) 435.

[6] a) FUERTES A., MIRATVILLES C., GONZALEZ-CALBET J., VALLET-REGI M., OBRADORS X., RODRIGUEZ-CARJAVAL J., *Physica C* **157** (1989) 529.

b) CALDES M.T., NAVARRO J.M., FONTCUBERTA J., CASAÑ N., OBRADORS X., RODRIGUEZ J., GONZALEZ-CALBET J.M., FUERTES A., MIRATVILLES C., *Chem. Mater.* **3** (1991) 844.

[7] CALDES M.T., HERVIEU M., RAVEAU B., FUERTES A., *J. Solid State Chem.* **97** (1992) 48

[8] CALDES M.T., HERVIEU M., RAVEAU B., FUERTES A., *J. Solid State Chem.* **98** (1992) 301.

[9] CALDES M.T., HERVIEU M., RAVEAU B., FUERTES A. *J. Solid State Chem.* **98** (1992) 48.
[10] CALDES M.T., FUERTES A., GOMEZ P., OBRADORS X., RODRIGUEZ J., *Physica C* **185-189** (1992) 681.
[11] CALDES M.T., Ph. D., University of Valencia (1992).
[12] CALDES M.T., FUERTES A., BRUNA L.L., OBRADORS X., FONTCUBERTA J., MARTINEZ B., PEREZ F., *J. Appl. Phys.* **70** (1991) 6184.
[13] STADELMANN P.A., *Ultramicroscopy* **21** (1987) 131.
[14] HEWAT E., *J. Micros. Spectrosc. Electron.* **13** (1988) 297.
[15] EFFENBERGER H., *J. Solid State Chem.* **73** (1988) 118.
[16] MATSUI Y., TAKEMAWA S., KISHIO K., UMEZONO A., NAKAMURA S., TSURUTA C. and IBE K., *Mat. Trans. JIM* **31** (1990) 595.
[17] TARASCON J.M., MICELI P.F., BARBOUX P., HWANG D.M., HULL G.W., GIROUD M., GREENE L.H., LE PAGE Y., MC KINNAN W.R., TSELEPSIS E., PLEIZIER G., EIBSCHUTZ M., NEUMAN D.A. and RHYNE J.J., *Phys. Rev. B* **39** (1989) 11587.
[18] TARASCON J.M., LE PAGE Y., MC KINNAN W.R., RAMESH R., EIBSCHUTZ M., TSELEPSIS E., WANG E. and HULL G.W., *Physica C* **167** (1990) 20.